Approximation of Single Scattering Properties of Ice and Snow Particles for High Microwave Frequencies

GUOSHENG LIU

Department of Meteorology, The Florida State University, Tallahassee, Florida

(Manuscript received 6 December 2003, in final form 27 February 2004)

ABSTRACT

As satellite high-frequency passive microwave data have recently become available, there is an increasing demand for an accurate and computationally efficient method to calculate the single scattering properties of nonspherical ice particles, so that it may be used in radiative transfer models for physical retrievals of ice water path and snowfall rate. In this study, two such approximations are presented for calculating the single scattering properties of three types of large ice particles: bullet rosettes, sector snowflakes, and dendrite snowflakes, for the frequency range of 85 to 220 GHz, based on results of discrete-dipole approximation (DDA) modeling. By analyzing the DDA modeling results, it is noted that, for nonspherical ice particles, the scattering and absorption cross sections and the asymmetry parameter have a magnitude between those of the two imaginary equal-mass spheres. One is a solid sphere, and the other is an ice–air mixed soft sphere whose diameter equals the particle's maximum dimension. Therefore, the first approximation involves substituting the single scattering properties of a nonspherical ice particle with those of an equal-mass sphere, which can be calculated by Lorenz–Mie theory, with an effective dielectric constant derived by mixing ice and air using the Maxwell–Garnett formula. The diameter of such an equal-mass sphere D is bigger than the diameter of the solid sphere D_0, but smaller than the particle's maximum dimension $D_{\max}$. Defining a softness parameter $\mathrm{SP} = (D - D_0)/(D_{\max} - D_0)$, it is found that the best-fit equal-mass sphere has an SP value of $0.2 \sim 0.5$ for calculating the volume scattering coefficient, depending on frequency and particle shape. At 150 GHz, the best-fit softness parameter is found to be $\sim 1/3$ when averaging over all particle shapes. For calculating the asymmetry parameter, the DDA model results show that the best-fit softness parameter is close to 0 (i.e., the same as the solid sphere) for frequencies higher than 150 GHz, while it is about 0.3 for 85.5 GHz. The second approximation presented is a polynomial fit to the scattering and absorption cross sections and the asymmetry parameter using the particle size parameter as an independent variable. For the scattering cross section, three fitting curves are derived for, respectively, rosettes, sector snowflakes, and dendrite snowflakes. For the absorption cross section, a single curve is used to fit all particle shapes. For the asymmetry parameter, two curves are derived, one for rosettes and one for snowflakes. The best-fit softness parameter for three particular frequencies (85.5, 150, and 220 GHz) and for three particle shapes in the first approximation, as well as the coefficients of the polynomial fit in the second approximation, are presented. After implementing these approximations in a radiative transfer model, radiative transfer simulations are carried out for a snowfall and an ice cloud case. The simulated brightness temperatures based on the two approximations agree with each other within 3 K, but are significantly different from those based on the solid- and the soft-sphere approximations.

1. Introduction

At frequencies higher than 80 GHz, scattering by cloud ice and snow particles becomes strong enough to be detected by spaceborne microwave radiometers. The scattering signatures have been utilized by several investigators to retrieve ice water path (Evans et al. 1998; Deeter and Evans 2000; Liu and Curry 2000; Weng and Grody 2000; Wang et al. 2001) and snowfall (Liu and Curry 1997; Katsumata et al. 2000). An essential requirement for developing a physically based retrieval algorithm is that the single scattering properties of the ice and snow particles (such as the particle's scattering and absorption coefficients and the scattering phase function) can be correctly calculated in the radiative transfer model. Due to the particles' nonspherical shapes, the modeling of the single scattering properties of the ice and snow particles has always been a difficult task. For the high microwave frequencies, two general approaches have so far been used. One is to treat the ice particles as objects with certain known shapes, such as columns, plates, rosettes, etc., and calculate their single scattering properties using techniques applicable to these shapes (e.g., Evans and Stephens 1995; O'Brien and Goedecke 1988). The second approach is to approximate the single scattering properties of a nonspherical ice particle by those of an imaginary sphere

Corresponding author address: Guosheng Liu, Department of Meteorology, The Florida State University, 404 Love Bldg., Tallahassee, FL 32306-4520.
E-mail: liug@met.fsu.edu

having the same mass, so that Lorenz–Mie theory may be applied. The imaginary sphere used so far is either a solid sphere with a smaller diameter than the ice particle's maximum dimension (Liu and Curry 2000; Evans et al. 2002, hereafter referred to as the solid-sphere approximation) or a low-density sphere with a diameter of the particle's maximum dimension, but with a reduced effective dielectric constant (Schols et al. 1999; Bennartz and Petty 2001; Zhao and Weng 2002), which is derived by mixing solid ice and air following a certain mixing formula (hereafter referred to as the soft-sphere approximation).

Neither approach is satisfactory for the purpose of developing a physically based algorithm to retrieve ice water path and snowfall rate. Although the first approach can accurately evaluate the radiative properties for given crystal shapes, the method is impractical because it is computationally intensive. The second approach is computationally efficient, but the validity of the approximation is unproven. As shown later in this study, single scattering properties differ significantly depending on whether a solid sphere or a low-density sphere is assumed, particularly for those particles with large maximum dimension and low density, such as snowflakes. Recognizing these problems, the goal of this study is to find a both accurate and computationally efficient method of calculating the single scattering properties of cloud ice and snow particles at high microwave frequencies. Since microwave radiation is sensitive only to large ice particles, the focus of the study will be on aggregates and snowflakes, which dominate the larger end of the size spectrum (Heymsfield et al. 2002b).

The following steps are taken to achieve the desired goal. First, we investigate how the numerically simulated single scattering properties differ when using a rigorous technique suitable for nonspherical particles as opposed to using simple Lorenz–Mie theory for imaginary equal-mass spheres. There are several published methods for calculating the scattering by nonspherical particles (Mishchenko et al. 2000), such as the T-matrix method (Mishchenko et al. 1996), the finite difference time domain method (Yang and Liou 1996, 1998), and the discrete-dipole approximation (DDA) method (Draine and Flatau 2000). The DDA model developed by Draine and Flatau (2000) is used in this study. The greatest advantage of the DDA method is its applicability to arbitrarily shaped particles, which enables us to study the scattering by ice particles with complicated shapes, such as dendrites. Based on the results of the model simulations, we then formulate two computationally efficient parameterizations, by which the ice particles' single scattering properties can be accurately computed.

High-frequency microwave data are available from several satellite and airborne sensors. The Special Sensor Microwave Water Vapor Sounder (SSM/T-2) and Advanced Microwave Sounding Unit—B (AMSU-B) possess channels ranging from 89 to 183 $\pm$ 7 GHz. The airborne Millimeter Wave Imaging Radiometer (Racette et al. 1996) has channels from 89 to 340 GHz. Additionally, channels ranging from 19 to 183 $\pm$ 7 GHz are available on Special Sensor Microwave Imager–Sounder (SSMIS). Ice scattering signatures from these instruments have been used for deriving ice water path and snowfall (Vivekanandan et al. 1991; Deeter and Evans 2000; Liu and Curry 2000; Weng and Grody 2000; Wang et al. 2001). In this study we investigate the radiative properties of ice crystals and snowflakes at these frequencies.

In section 2, we briefly describe the DDA model, the ice particles and snowflakes designed for the DDA model simulations, and the single scattering properties simulated by the DDA model. An equal-mass sphere approximation is proposed in section 3, and a polynomial fit approximation is introduced in section 4. Radiative transfer modeling based on the two approximations are carried out in section 5. Finally, the results are summarized in section 6.

2. Modeling the single scattering properties of ice and snow particles

a. The discrete-dipole approximation

The DDA model developed by Draine and Flatau (2000) is used to compute the single scattering parameters of the ice and snow particles. The DDA is a general method for computing the scattering and absorption by a particle of arbitrary shape (Purcell and Pennypacker 1973), and has been used by many researchers for studying the scattering by interstellar grains and ice particles (e.g., Draine 1988; Evan and Stephens 1995). Simply stated, the DDA is an approximation of the continuum target by a finite array of polarizable points. The points acquire dipole moments in response to the local electric field. The dipoles also interact with one another via their electric fields. The principal advantage of the DDA is that it is flexible regarding the geometry of the target. The limitation is that the interdipole spacing must be sufficiently small compared to the wavelength in order to obtain desired accuracy, which requires large computer memory and long computation time for large particles.

The implementation of the Draine and Flatau DDA model approximates the targets by an array of polarizable points that are located on a cubic lattice (Draine 1988). The lattice spacing d should satisfy the criterion: $|m|kd < 0.5$ (Draine and Flatau 2000), where m is the complex refractive index of the target material, $k = 2\pi/\lambda$ is the angular wavenumber, and λ is the wavelength. We use a variable d for different particle sizes in this study, while ensuring the above criterion being always met. Assuming the polarizability and the dipole moment for the jth dipole are α_j and $\mathbf{P}_j$, respectively, the DDA model seeks to find the solution for a self-consistent set of dipole moments; that is,

$$\mathbf{P}_j = \alpha_j \left(\mathbf{E}_{\text{inc},j} - \sum_{j \neq i} \mathbf{A}_{ji} \mathbf{P}_i \right), \quad (1)$$

where $\mathbf{E}_{\text{inc},j}$ is the electric field at the position j due to the incident plane wave, and $-\mathbf{A}_{ji}\mathbf{P}_i$ is the contribution to the electric field at the position j due to the dipole at position i. The $\mathbf{A}_{ji}$ can be expressed by a function of angular wavenumber k and the relative position of the dipoles j and i. The mathematical expression of $\mathbf{A}_{ji}$ can be found in Draine and Flatau (1994). Defining $\mathbf{A}_{ij} = \alpha_j^{-1}$ reduces the scattering problem to finding the dipole moments $\mathbf{P}_j$ that satisfy a system of complex linear equations:

$$\sum_{i=1}^{N} \mathbf{A}_{ji} \mathbf{P}_i = \mathbf{E}_{\text{inc},j}, \quad (2)$$

where N is the total number of dipoles. Once (2) has been solved for the unknown dipole moment $\mathbf{P}_j$, the single scattering parameters including the scattering and absorption cross sections C_{ext} and C_{abs}, the asymmetry parameter, and the phase matrix of scattering may be evaluated according to Draine (1988).

One of the major differences among different implementations of the DDA is how to prescribe the polarizability [α_j in (1)] of the point dipoles used to represent the target. Draine and Goodman (1993) chose the dipole polarizability based on a lattice dispersion relation so that an infinite lattice with finite spacing will mimic a continuum with the specified dielectric constant function. They compared this prescription with several other choices of the dipole polarizability published in the literature, and showed that the most accurate results are obtained when the lattice dispersion relation is used to set the polarizabilities. In this study, we use the Draine and Goodman (1993) relation to evaluate polarizability, although the Draine and Flatau (2000) DDA model allows the choice of several other options. A validation by comparing DDA with Lorenz–Mie results for spheres has been done. It is found that the scattering cross sections from the two methods agree with each other within 1%, and the phase functions from the two methods are almost identical, for $|m|kd < 0.45$ at 150 GHz. A more detailed validation may be found in Draine and Flatau (1994).

b. Cloud ice particles and snowflakes

Due to the long wavelength of microwave radiation, only scattering signals from large ice particles are strong enough to be detected by a microwave sensor. For this reason, our main focus will be on the larger end of the ice particle size spectrum, specifically, rosettes and snowflakes. As pointed by Heymsfield et al. (2002b), in the midlatitude anvils formed by strong convection and even in deep, synoptically generated cirrus, aggregates dominate the larger end of the size spectrum (Kajikawa and Heymsfield 1989). Tropical-anvil ice particle data collected from field experiments have indicated that planar crystals and aggregates are prevalent in anvils. Additionally, Heymsfield et al. (2002b) indicated that particle habits above about 100 μm consisted almost exclusively of rosettes and aggregates of rosettes for a case conducted in Oklahoma. Therefore, we will use rosettes (three to six bullets) to represent ice particles in clouds. For snowflakes, a sector- and a dendrite-type particle are used as described below.

In deriving the single scattering properties, both rosettes and snowflakes are assumed to be randomly oriented in space. The orientational average of a quantity Q can be calculated by (Draine and Flatau 2000)

$$\langle Q \rangle = \frac{1}{8\pi^2} \int_0^{2\pi} d\beta \int_{-1}^{1} d\cos\theta \int_0^{2\pi} d\varphi Q(\beta, \theta, \varphi), \quad (3)$$

where β, θ, and φ are the three angles to describe the orientation of the ice particle in the Draine and Flatau DDA model. All DDA model-calculated quantities presented in the following sections are orientationally averaged, although we will not put the bracket "$\langle\ \rangle$" around them for simplicity.

1) ROSETTES

Rosettes are represented by aggregates of hexagonal columns connected at the center. For this study, we construct rosettes with three to six bullets. The three- and four-bullet rosettes consist of three and four coplanar columns that display a "$\perp$" and a "$+$" shape, respectively. The five- or six-bullet rosette is constructed by adding one or two columns to a four-bullet rosette in the direction perpendicular to the other four bullets. Columns that make up the same rosette have the same length and aspect ratio. But the aspect ratios for rosettes with a different number of bullets are different depending on the area ratio–maximum dimension relations given below. To determine the aspect ratio of the columns, we use a relationship between the maximum dimension D_{max} and the area ratio A_r derived by Heymsfield and Miloshevich (2003):

$$A_r = aD_{\text{max}}^b, \quad (4)$$

where $a = 0.125$ and $b = -0.351$ (in cgs units), which are the values determined for rosettes based on Cloud Particle Imager (CPI) measurements. Ratio A_r is the projected area of an ice particle normalized by the area of a circle with diameter D_{max}. By letting (4) hold while D_{max} varies, the aspect ratio of the columns can be determined. In Fig. 1a, the images of the three-, four-, five-, and six-bullet rosettes for $D_{\text{max}} = 1000$ μm are shown, with the small circles indicating the individual dipoles.

2) SNOWFLAKES

Two types of snowflakes are considered. The first type (type A) is a sectorlike particle, represented by three

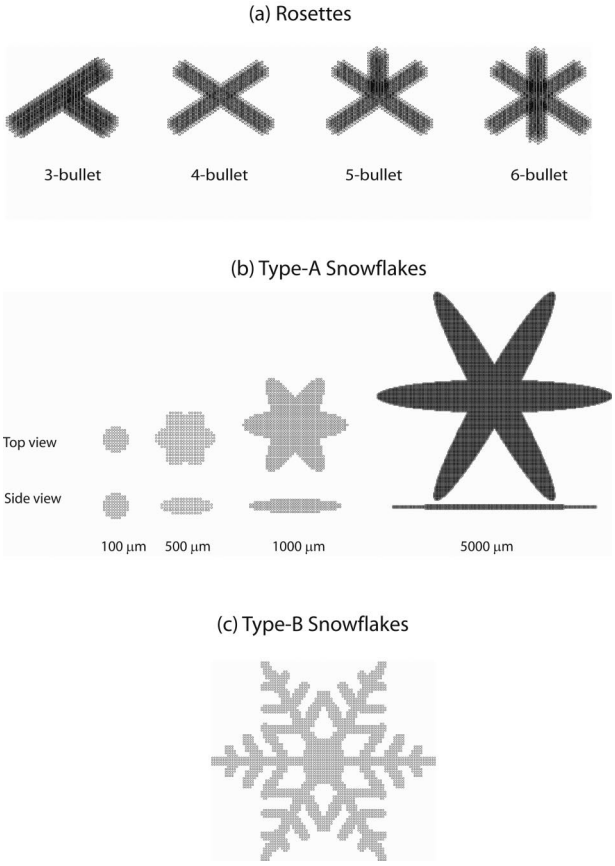

FIG. 1. Shapes of (a) rosettes, (b) type-A snowflakes, and (c) type-B snowflakes used in the DDA model simulations. Note the scales in (b) are not the same for particles with different sizes for viewing purposes (condensed for larger particles).

identical ellipsoids that share the same center, and whose longest axes are orientated 60° apart. Given the maximum dimension of a snowflake $D_{\max}$, the diameters of an ellipsoid in the other two dimensions are determined by the following relations (cgs units):

$$A_r = 0.261 D_{\max}^{-0.377}, \quad \text{and} \tag{5a}$$

$$\rho_e = 0.015 A_r^{1.5} D_{\max}^{-1.0}, \tag{5b}$$

where ρ_e is effective density defined as the mass divided by the volume of a circumscribed sphere. The relation (5a), given by Heymsfield and Miloshevich (2003), was derived based on surface measurement data for aggregate planar crystals (Kajikawa 1982). The relation of (5b) was derived by Heymsfield et al. (2002b) for aggregates. Combining (5a) and (5b) makes ρ_e approximately proportional to $D_{\max}^{-1.6}$, similar to the relation given by Magono and Nakamura (1965). The top and side view of the images for $D_{\max}$ = 100-, 500-, 1000-, and 5000-μm type-A snowflakes are shown in Fig. 1b. A more sophisticated mathematical expression of this type of snowflakes was given by Wang (1997).

The type-B snowflake is a dendrite as shown in Fig. 1c (top view), similar to the dendrite used by O'Brien and Goedecke (1988). As the particle size increases, the area ratio A_r does not change. To determine the depth of the dendrites, (5b) is used, which results in a nearly constant value of $\sim$70 μm for the depth of particles with maximum dimension from 340 to 12 000 μm. The difference between the two types of snowflakes is that the ice volume is concentrated on six main branches in type-A, while it spreads more uniformly in the basal plane in type-B snowflakes.

c. DDA model results

In this study, the following radiative quantities are defined and evaluated: the normalized absorption cross section $C_{\text{abs}}/\pi r_{\text{eff}}^2$, where C_{abs} is the absorption cross section and r_{eff} is an ''effective'' radius of the ice/snow particle defined so that the mass of the particle equals $(4/3)\pi r_{\text{eff}}^3 \rho_i$ (ρ_i = 0.916 g cm^{-3} is the density of solid ice); the normalized scattering cross section $C_{\text{sca}}/\pi r_{\text{eff}}^2$, where C_{sca} is the scattering cross section; the asymmetry parameter g; and the normalized phase function $P(\Theta)$, where Θ is the angle between incidence and emergence waves. Note that, for solid spheres the normalized scattering (absorption) cross section is the conventionally called scattering (absorption) efficiency. As mentioned earlier, all quantities are orientationally averaged assuming that particles are randomly orientated in space. The Draine and Flatau DDA model is used for nonspherical particles, while the Lorenz–Mie theory is used for spheres of an ice–air mixture with the Maxwell–Garnett mixing formula assuming that ice is the matrix and air is the inclusion (Bohren and Battan 1982). We first discuss the single scattering properties at 150 GHz and at temperature of -10°C. The frequency and temperature dependences are then discussed in later sections.

1) SINGLE SCATTERING PROPERTIES OF ROSETTES

In Fig. 2, we show the normalized cross sections and asymmetry parameter at 150 GHz as a function of $D_{\max}$ for three- and six-bullet rosettes calculated using the DDA model, as compared with those calculated using Lorenz–Mie theory assuming either an equal-mass solid sphere with a radius r_{eff} (hereafter referred to as a solid sphere) or an equal-mass low-density sphere with a diameter $D_{\max}$ (hereafter referred to as a soft sphere). Note that at a given $D_{\max}$, the normalized cross sections for the solid sphere is the cross sections of a solid sphere with a radius of r_{eff} normalized by πr_{eff}^2, not the cross sections of a solid sphere with a diameter of $D_{\max}$ normalized by $\pi(D_{\max}/2)^2$. So, the comparisons in the figure are among those particles with the same volume of ice and their scattering and absorption cross sections are normalized by πr_{eff}^2. Comparing among these figures, it is noticed that the single scattering parameters of the

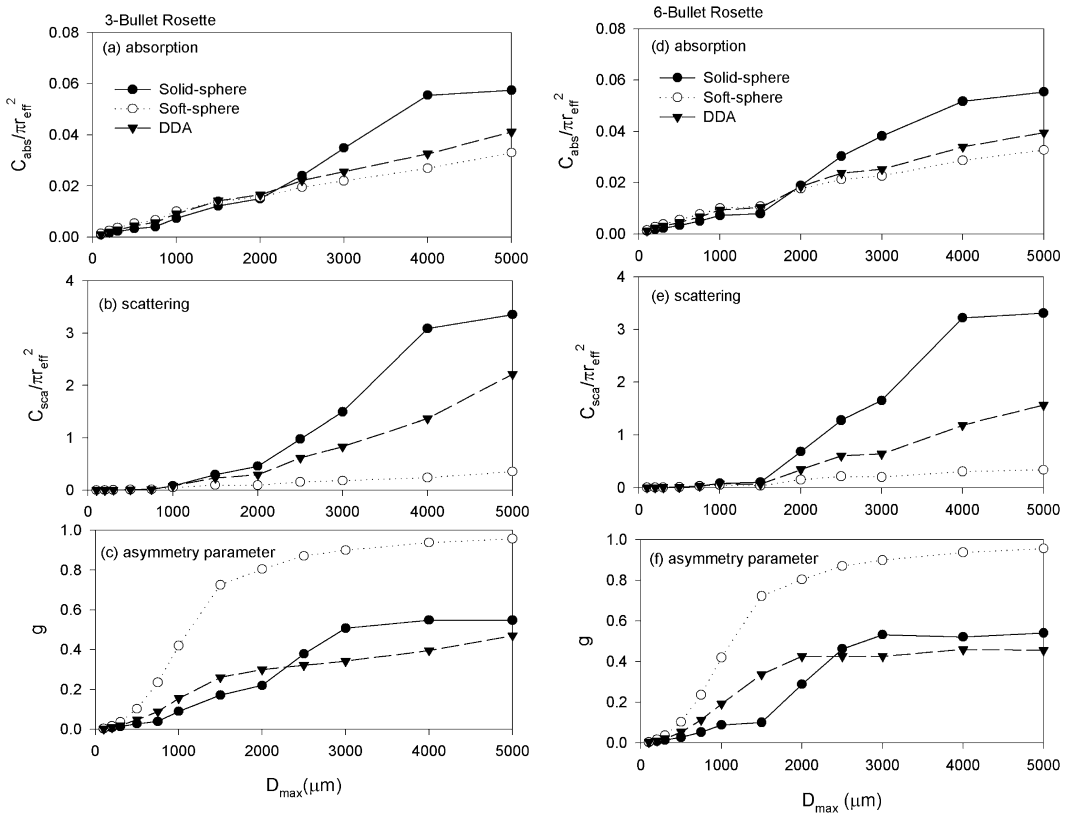

FIG. 2. Single scattering parameters for (a)–(c) three- and (d)–(f) six-bullet rosettes simulated by DDA model (long dashed lines), and approximated by the solid spheres (solid lines) and the soft spheres (dotted lines).

three- and six-bullet rosettes are quite similar. So are those of four- and five-bullet rosettes (not shown).

We observe the following characteristics from the figures, which serve as the basis for our parameterization in the next sections. First, the normalized absorption cross section is about two orders smaller than the normalized scattering cross section manifesting the small magnitude of the imaginary part of the dielectric constant of ice. So, we may mainly concentrate on parameterization for scattering. Second, the values of the cross sections from the DDA model fall between those of the solid- and the soft-spheres calculated by Lorenz–Mie theory. The differences among the three curves are small for particles with D_{max} smaller than 1500 μm, but increase as the particle size becomes larger. Third, the value of the asymmetry parameter is much closer to the solid spheres' than to the soft spheres', particularly when the ice particles are large. A closer look at the angular distribution of the scattered energy is shown in Fig. 3 by the phase functions for the six-bullet rosettes with $D_{max} = 750$ μm and $D_{max} = 2500$ μm. The phase functions for the solid and the soft spheres are also shown in the figure for comparison. For $D_{max} = 750$ μm, the phase function from the DDA model falls between the solid and soft spheres'. For $D_{max} = 2500$ μm, the DDA phase function is between the solid and soft spheres' for the directions of $\Theta = 0$–$90°$, but is slightly larger than the other two at the directions of $\Theta > 90°$. However, scattering energy distributed in the backward direction is much smaller than that in the forward direction for the large particles.

2) SINGLE SCATTERING PROPERTIES OF SNOWFLAKES

Similar to Figs. 2 and 3 for rosettes, we plotted $C_{abs}/\pi r_{eff}^2$, $C_{sca}/\pi r_{eff}^2$, g, and $P(\Theta)$ at 150 GHz in Figs. 4 and 5 for the two types of snowflakes as described in section 2b(2). The maximum dimension D_{max} is up to 10 000 μm in these plots. In Fig. 5, the phase functions are for particles with maximum dimension of 1000 and 5000 μm for type A, and 936 and 4291 μm for type B snowflakes. The general conclusions drawn from the results for rosettes appear to also apply here to the snowflakes. That is, 1) $C_{abs}/\pi r_{eff}^2$ is about two orders smaller than $C_{sca}/\pi r_{eff}^2$; 2) the values of $C_{abs}/\pi r_{eff}^2$ and $C_{sca}/\pi r_{eff}^2$ calculated from the DDA model are between those of the equal-mass solid and soft spheres'; and 3) g is closer to that for solid spheres, and g calculated by the DDA model is between those for the solid and soft spheres. For small snowflakes ($D_{max} \sim 1000$ μm), the phase function from the DDA model is between the equal-mass

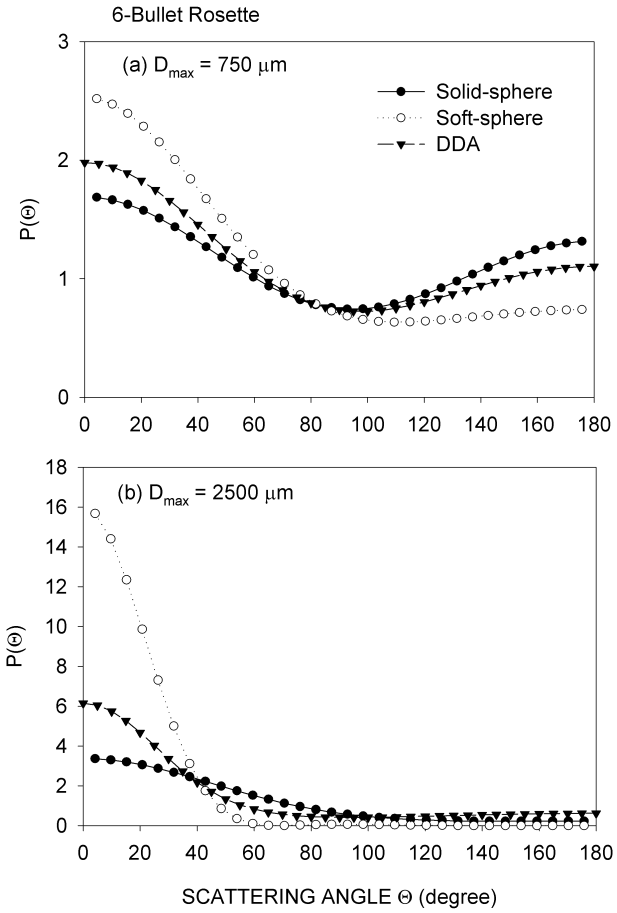

FIG. 3. Phase functions for six-bullet rosettes with maximum dimensions of (a) 750 and (b) 2500 μm. Dashed lines are DDA model results. Solid and dotted lines are, respectively, for the solid- and the soft-sphere approximations.

solid and soft spheres. For large snowflakes ($D_{max} \sim 5000$ μm), the DDA phase function is between those of the solid and soft spheres only in the directions with small Θs.

3) TEMPERATURE DEPENDENCE

The complex refractive index of ice only weakly depends on temperature at the microwave spectrum, particularly the real portion of the index. As a result, the single scattering properties do not have significant temperature dependence. Our calculations show that at 150 GHz the values of C_{sca} for type-A snowflakes vary less than 0.2% when the temperature decreases from 0° to −20°C, a difference smaller than the precision of the DDA model itself. For the absorption cross section, the relative difference is larger (~50%) due to the greater relative change in the imaginary portion of the refractive index. However, as mentioned earlier, C_{abs} is roughly two orders smaller than C_{sca} for the same ice particle; our focus will be mainly on scattering in this study. Therefore, we simply use temperature of −10°C for all the calculations in the subsequent sections.

3. Approximation by equal-mass spheres

As shown in the previous section, the single scattering parameters of the nonspherical particles fall between those of the solid- and soft-spheres. Therefore, a straightforward solution to simplify the calculation of these parameters is to use the single scattering properties of an equivalent sphere to represent those of a nonspherical particle, so that Lorenz–Mie theory can be employed. The equivalent sphere should have the same mass as the nonspherical particle, and have an effective density between the density of solid ice and that of the soft-sphere. Let's define a ''softness parameter'' SP as follows:

$$\mathrm{SP} = \frac{D - D_0}{D_{\max} - D_0}, \tag{6}$$

where D, D_0, and D_{max} are, respectively, the diameters of the equivalent sphere, the solid sphere, and the soft sphere (or the maximum dimension of the particle). That is, SP = 0 corresponds to the solid sphere and SP = 1 corresponds to the soft sphere. Our task is then to find the most appropriate value of SP, so that the equivalent sphere with this SP has the closest single scattering properties to those of the nonspherical particle. A different kind of spherical approximation was proposed by Grenfell and Warren (1999), in which the volume-to-surface-area ratio is preserved while representing one nonspherical particle by multiple independent spheres.

a. Individual particles

In Fig. 6, we show the DDA model-calculated normalized scattering cross sections, represented by thick lines with solid circles, at 150 GHz for five-bullet rosettes, type-A snowflakes, and type-B snowflakes, along with those calculated by the equivalent spheres with various SPs. As particle size increases, the values of the normalized scattering cross section increase for all of the particles but with different rates. For five-bullet rosettes, the normalized scattering cross section calculated by DDA varies similarly to the normalized scattering cross section of an equivalent sphere with SP = 0.25 ~ 0.3. For type-A snowflakes, the DDA derived normalized scattering cross section follows the normalized scattering cross section of an equivalent sphere with SP = 0.2 And for type-B snowflakes, the normalized scattering cross section of an equivalent sphere with SP = 0.3 ~ 0.4 appears to be a good approximation for the DDA model calculated one. The values of SP of the equivalent spheres that best fit the DDA-calculated normalized scattering cross sections are calculated by minimizing the root-mean-squared differences and are shown in Fig. 7. Also shown in this figure are the differences between the normalized scattering cross sec-

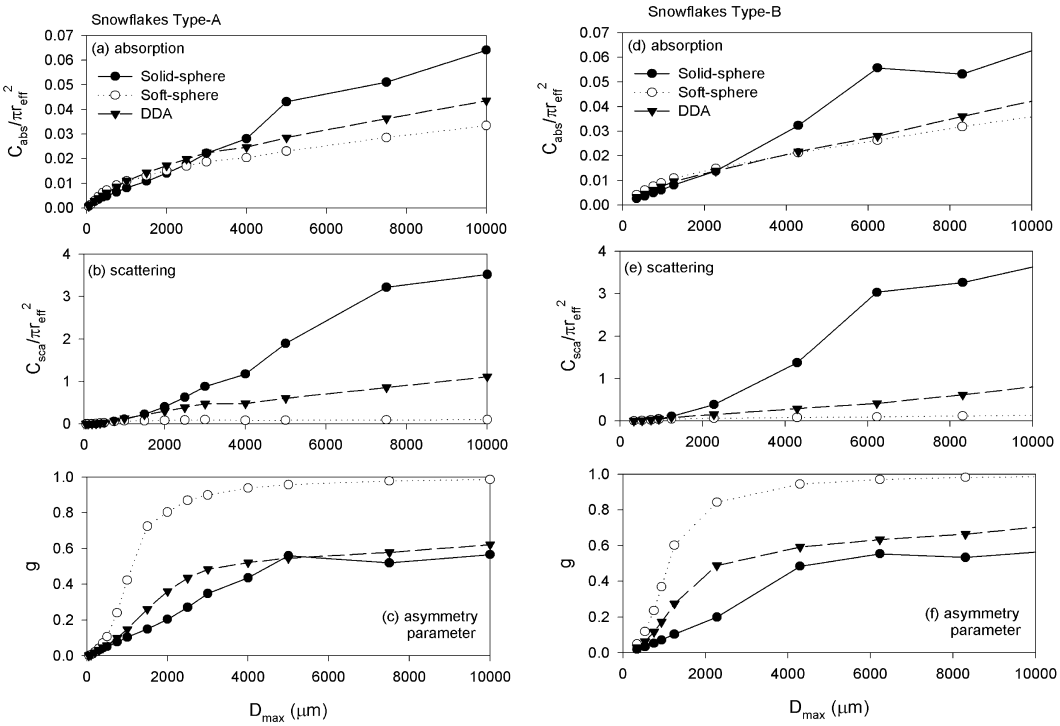

FIG. 4. Single scattering parameters for (a)–(c) type-A and (d)–(f) type-B snowflakes simulated by DDA model (dashed lines), and approximated by the solid spheres (solid lines) and the soft spheres (dotted lines).

tions of the equal-mass spheres with SP = 0 and SP = 1 (denoted by $\Delta C_{sca}/\pi r_{eff}^2$). For particles with D_{max} smaller than 1000 μm, the normalized scattering cross sections calculated from all SPs are close to each other ($\Delta C_{sca}/\pi r_{eff}^2$ is small). So, we did not show the best-fit SP for these particles. As particle size increases, the differences among the normalized scattering cross sections of the equivalent spheres with different SPs increase, too. But the SP value with which the $C_{sca}/\pi r_{eff}^2$ of an equivalent sphere best fits the DDA result becomes less variable. This value is 0.2 ~ 0.3 for rosettes, ~0.2 for type-A snowflakes, and 0.3 ~ 0.4 for type-B snowflakes. The best-fit SP for type-A snowflakes is somewhat smaller than that for type-B snowflakes, reflecting the difference in spatial mass distribution between the sectorlike and the dendritelike snowflakes. Interestingly, the values of the best-fit SPs for all the three ice shapes are surprisingly similar, ranging from 0.2 to 0.4, except for the particles with relatively small size ($D_{max} < 2000$ μm).

Next, we compare the phase functions calculated by the DDA model with those approximated by the equivalent spheres using various SPs. We select the particle sizes of 750 and 4000 μm for five-bullet rosettes, 1000 and 5000 μm for type-A snowflakes, and 936 and 6227 μm for type-B snowflakes. The results are shown in Fig. 8. For smaller particles, the phase function calculated from the DDA model follows the pattern of an equivalent sphere's distribution. For example, the $P(\Theta)$ of 750-μm five-bullet rosette is very similar to the $P(\Theta)$ of an equivalent sphere with SP = 0.5, the $P(\Theta)$ of 1000-μm type-A snowflake resembles that of an equivalent sphere with SP = 0.25, and the $P(\Theta)$ of the 936-μm type-B snowflake has a similar phase function to an equivalent sphere with SP = 0.5. For large particles, the angular distribution of the scattering departs from the pattern of any equivalent sphere's phase function. At small scattering angles ($\Theta < 10°$), the DDA $P(\Theta)$ is close to the $P(\Theta)$ of an equivalent sphere with an SP ranging from 0.2 to 0.4, depending on the particle shape. As the scattering angle increases, the DDA $P(\Theta)$ decreases in a faster rate than the $P(\Theta)$ for equivalent spheres calculated based on Lorenz–Mie theory. As an alternative to fitting the phase function itself, in this study we choose to find the best-fit SP values of the asymmetry parameter, so that the phase function may then be approximated by a known function such as the Henyey–Greenstein phase function (Henyey and Greenstein 1941). Similar to Fig. 7, Fig. 9 shows the best-fit SPs values based on the asymmetry parameters, together with the difference of the asymmetry parameters when SP = 0 and SP = 1. An SP value of 0.2 to 0.4 is suitable for particles with $D_{max} < 2000$ μm, while the best-fit SP rapidly decreases to 0 (i.e., that of the solid sphere) as particle size increases.

b. Integration over a size distribution

Since ice particles with various sizes coexist in a cloud/snowfall volume, the best-fit SP values to be used in the

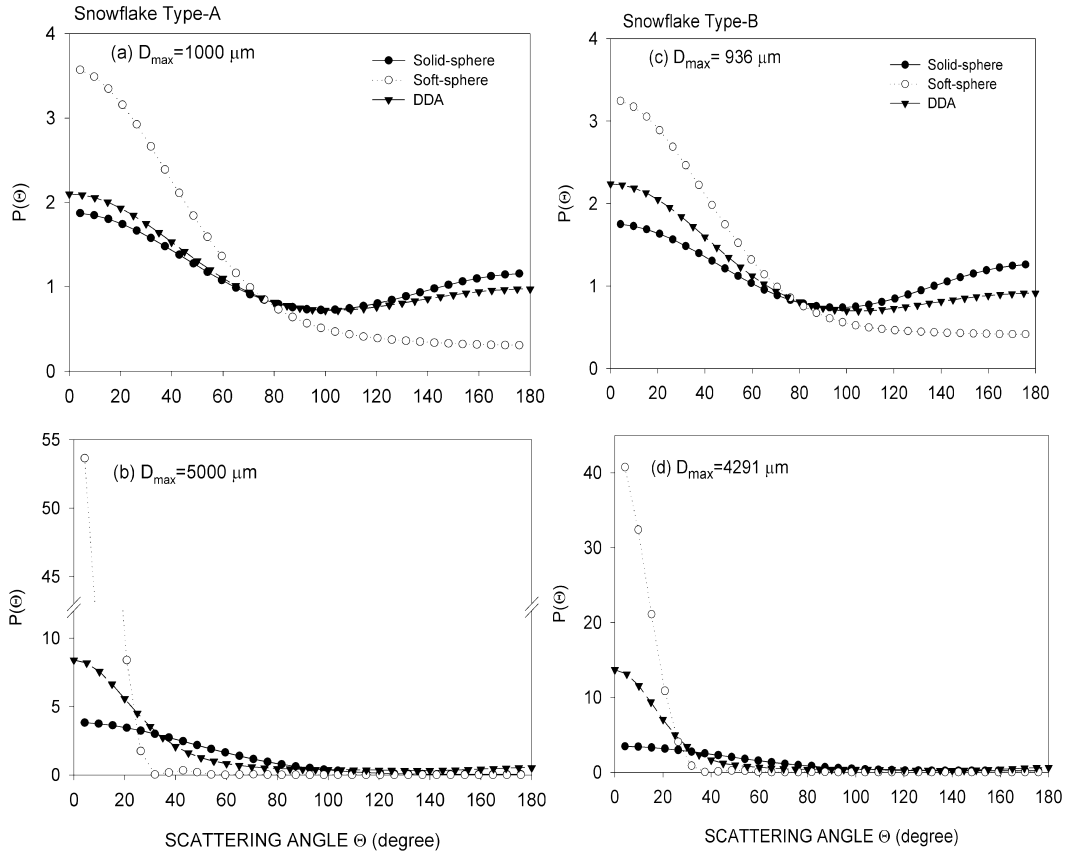

FIG. 5. Phase functions for (a), (b) type-A and (c), (d) type-B snowflakes. Dashed lines are DDA model results. Solid and dotted lines are, respectively, for the solid- and soft-sphere approximations.

approximation by equivalent spheres may be evaluated by taking into account the particles' size distribution. For this purpose, we use a gamma size distribution for rosettes and an exponential distribution for snowflakes. The gamma size distribution can be written as $N(D_{\max}) = N_{0\Gamma} D_{\max}^{\mu} e^{-\lambda_\Gamma D}$, where $N(D_{\max})$ is the number of particles with the maximum dimension $D_{\max}$. Heymsfield et al. (2002a) parameterized the values of the intercept ($N_{0\Gamma}$), slope (λ_Γ), and dispersion (μ) in terms of the ambient temperature T and ice water content (IWC). We use $T = -10$°C to derive these parameters. For snowflakes, we use the exponential distribution, $N(D_{\text{melt}}) = N_{0s} e^{-\lambda_s D_{\text{melt}}}$, given by Sekhon and Srivastava (1970), where N_{0s} and λ_s are functions of snowfall rate (R_s), and D_{melt} is the diameter of a melted water drop. The volume scattering coefficient σ_{sca}, and the volume averaged asymmetry parameter $\overline{g}$ can be expressed by

$$\sigma_{\text{sca}} = \int N(D) C_{\text{sca}}(D)\, dD, \quad \text{and} \tag{7}$$

$$\overline{g} = \frac{1}{\sigma_{\text{sca}}} \int N(D) C_{\text{sca}}(D) g(D)\, dD. \tag{8}$$

The best-fit SP values concerning σ_{sca} are shown in Fig. 10, when varying ice water content from 0.05 to 0.5 g m^{-3} (for rosettes), and snowfall rate from 0.5 to 5 mm h^{-1} (for snowflakes). For rosettes, the best-fit SPs range from 0.25 to 0.4 with an average value of 0.33. The best-fit SP is ~0.2 for type-A (sectorlike) snowflakes, and ~0.33 for type-B (dendritelike) snowflakes. The averaged best-fit SP over all particle shapes considered here is ~1/3. The best-fit SP values concerning $\overline{g}$ are also investigated using the above size distributions and are shown in Fig. 11. As discussed earlier, for large particles, the DDA asymmetry parameter is close to that of the solid sphere. Since large particles weight heavily in the averaging [ref. (8)], the best-fit SPs are very close to 0 for all the particle shapes considered here. Therefore, in the case of 150 GHz, we may evaluate the averaged asymmetry parameter using a solid sphere.

c. Frequency dependence

To study the frequency dependence of the scattering properties, DDA modeling at two more frequencies, 85.5 and 220 GHz, is also carried out. Table 1 lists the best-fit SPs at 85.5, 150, and 220 GHz, applying the size distributions given in section 3b. As seen from Figs. 10 and 11, the best-fit SPs vary little with ice water content or snowfall rate. Therefore, we only show the

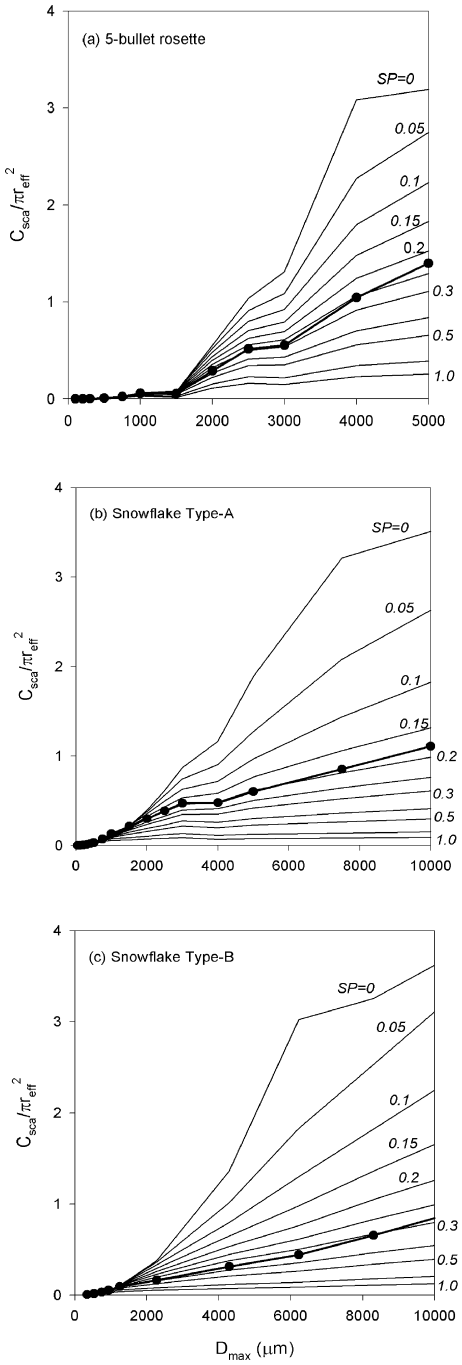

FIG. 6. Comparison of the DDA model-calculated normalized scattering cross sections (thick lines with solid dots) with those of equivalent spheres with various softness parameters for (a) five-bullet rosettes, (b) type-A snowflakes, and (c) type-B snowflakes.

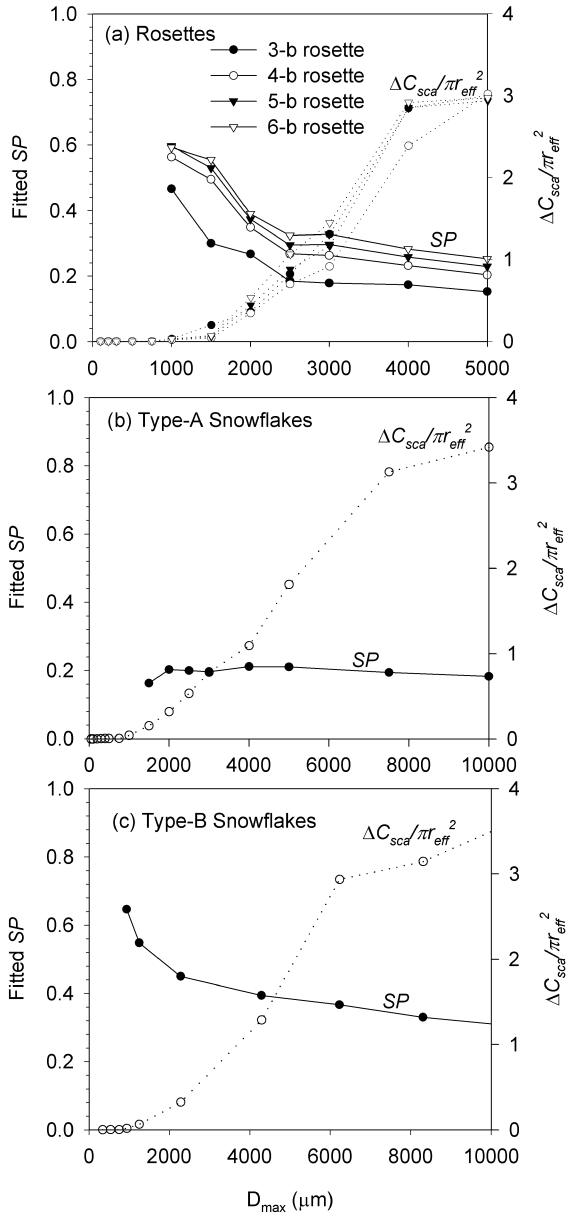

FIG. 7. Best-fit SP values concerning the normalized scattering cross sections $C_{sco}/\pi r_{eff}^2$ for (a) rosettes, (b) type-A snowflakes, and (c) type-B snowflakes. Also shown are the differences between $C_{sco}/\pi r_{eff}^2$ values when assuming equivalent spheres with SP = 0 and SP = 1.

best-fits for ice water content of 0.2 g m^{-3} or snowfall rate of 2 mm h^{-1}. Clearly, there is a frequency dependence of the best-fit SPs—a higher frequency corresponds to a smaller value of the best-fit SP. Using the best-fits derived by σ_{sca}, the averaged SPs at 85.5, 150, and 220 GHz are 0.54, 0.34, 0.26 for rosettes, and 0.33, 0.27, and 0.22 for snowflakes. For best-fit SPs derived by $\overline{g}$, SP = 0 is suitable for frequencies higher than 150 GHz, while it is found that SP = 0.34 for rosettes and SP = 0.11 for snowflakes at 85.5 GHz.

4. Approximation by curve fitting

Another approach for the approximation is to parameterize the single scattering properties by expressing them as a function of particle size, based on the results

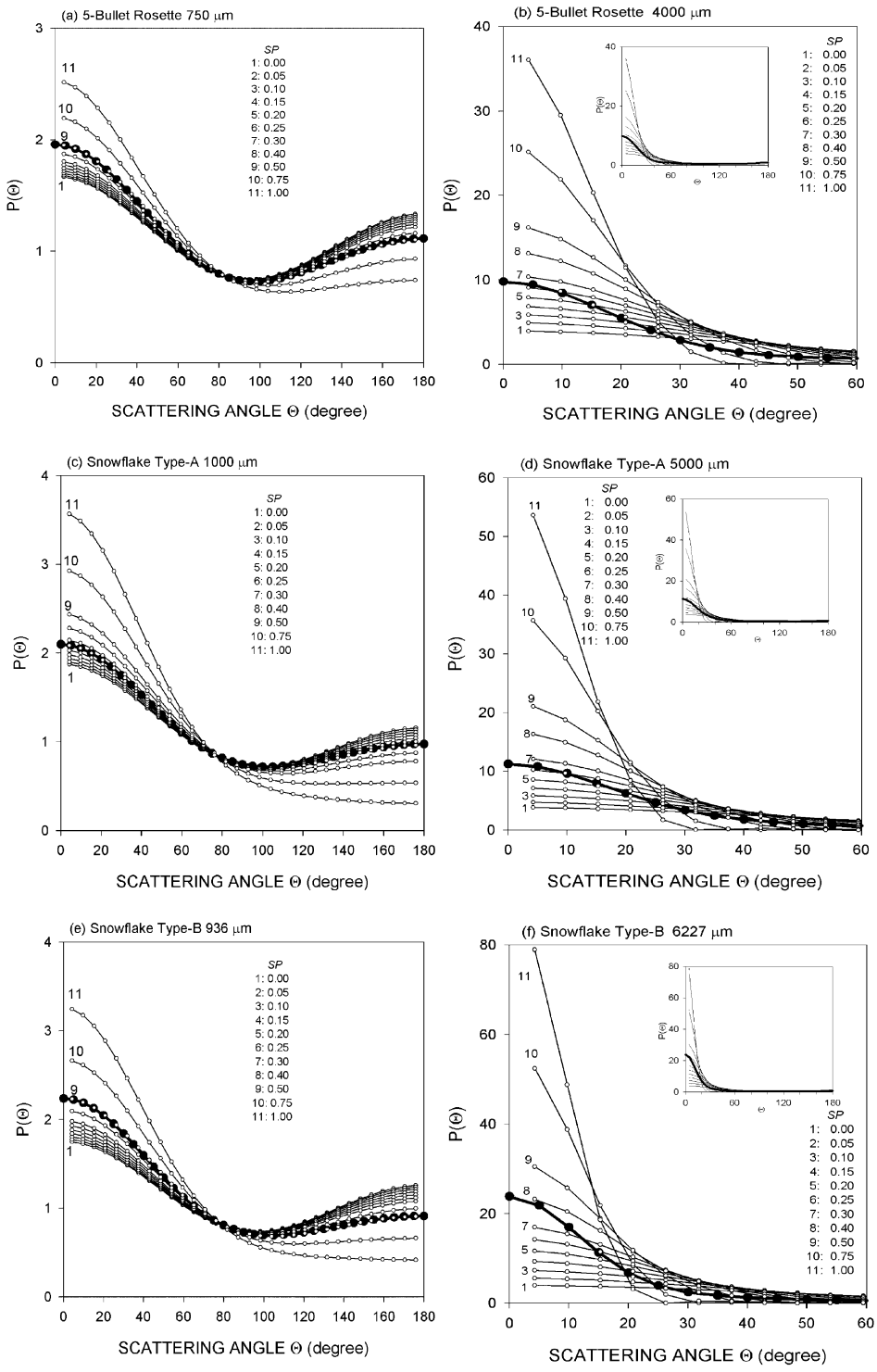

FIG. 8. Comparison of DDA model-calculated phase functions with those of equivalent spheres with various softness parameters for (a) 750-μm five-bullet rosette, (b) 4000-μm rosette, (c) 1000-μm type-A snowflake, (d) 5000-μm type-A snowflake, (e) 936-μm type-B snowflake, and (f) 6227-μm type-B snowflake. For large particles (right), the insertions show the scattering angles ranging from 0° to 180°, while the main figures show the scattering angles less than 60°.

calculated by the DDA model. The parameterized properties can then be used in radiative transfer models. In this study, we choose the following polynomial form for the fitting functions:

$$\frac{C_{\text{sca}}}{\pi r_{\text{eff}}^2} = \sum_{n=1}^{3} a_n x^n, \tag{9a}$$

$$\frac{C_{\text{abs}}}{\pi r_{\text{eff}}^2} = \sum_{n=1}^{3} b_n x^n, \tag{9b}$$

$$g = \sum_{n=0}^{3} c_n x^n, \tag{9c}$$

where $x = 2\pi r_{\text{eff}}/\lambda$ is the size parameter defined by the effective radius of the ice particle, and a_n, b_n, and c_n are coefficients of the fitting curves. We could not find a suitable form to parameterize the phase function. Here, we provide a parameterization of the asymmetry parameter as shown in (9c). In these fitting functions, we use size parameter x as an independent variable. Recalling that the relation between r_{eff} and the maximum dimension depends on particle shapes, the effective density of the particles is implicitly included in these fitting functions.

In this fitting, we combine DDA results for all three frequencies: 85.5, 150, and 220 GHz. Figure 12 shows the scatterplot of $C_{\text{sca}}/\pi r_{\text{eff}}^2$, $C_{\text{abs}}/\pi r_{\text{eff}}^2$, and g versus x, together with the fitting curves. The coefficients of the fitting curves are listed in Table 2. For the normalized scattering cross section, we use three fitting functions, respectively, for rosettes, type-A snowflakes and type-B snowflakes. For the normalized absorption cross section, the spread of data points among different particle shapes is relatively small; a single fitting curve is used for all particle shapes. For the asymmetry parameter, the spread between the two snowflake types is relatively small; one fitting curve is used for both snowflake types. Therefore, we provide one fitting curve for rosettes and one for snowflakes. It must be cautioned that the polynomial fit works only within the range of x used for the regression, which is 0 to ~3 for rosettes and 0 to ~4 for snowflakes. Any extrapolation will result in a significant error.

It is noticed that differences of the single scattering properties among the various rosettes are significantly smaller; this is also true of the difference of the single scattering properties between the two types of snowflakes. This similarity may be partially due to the fact that ice particles in this study are assumed to be randomly orientated in space. The random orientation has the effect that the single scattering properties are more sensitive to the mass of the ice and less sensitive to the texture of the particles.

5. Radiative transfer modeling

To demonstrate the usefulness of the approximation methods presented in this study, we carry out radiative transfer simulations for two cases: a tropical thick ice cloud and a high-latitude snowfall. Both approximation methods are implemented in a four-stream radiative transfer model developed by Liu (1998), in which a Henyey–Greenstein phase function is used. The best-fit SPs values for σ_{sca} and $\overline{g}$ listed in Table 1 are used in the equal-mass sphere approximation, and fitting curves represented by (9) and Table 2 are used in the polynomial fitting approximation.

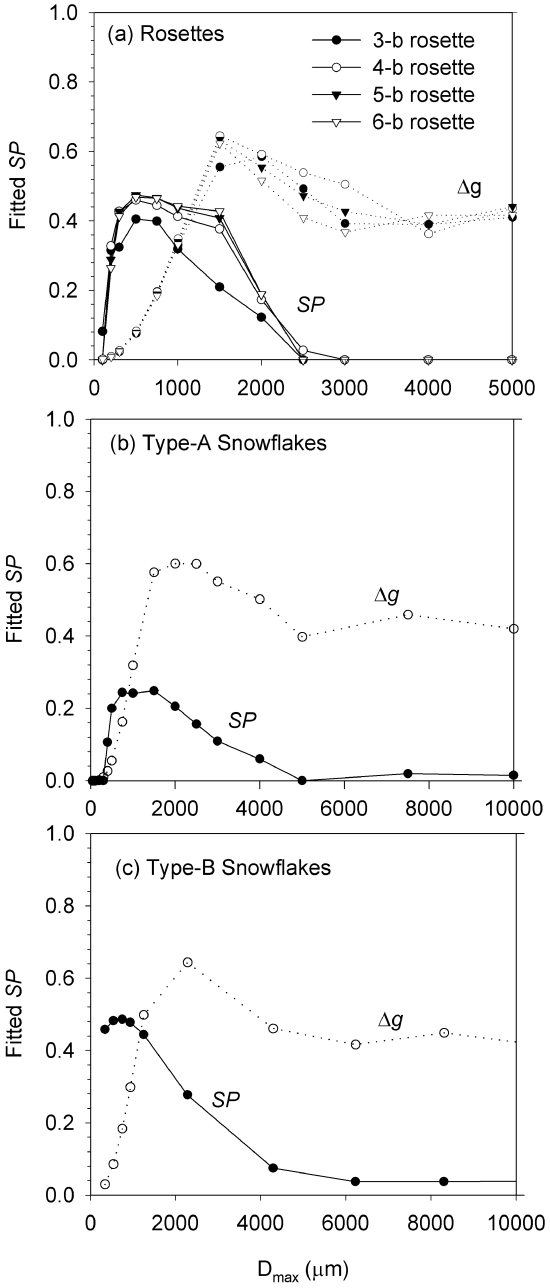

FIG. 9. Best-fit SP values concerning asymmetry parameters for (a) rosettes, (b) type-A snowflakes, and (c) type-B snowflakes. Also shown are the differences between the asymmetry parameters when assuming equivalent spheres with SP = 0 and SP = 1.

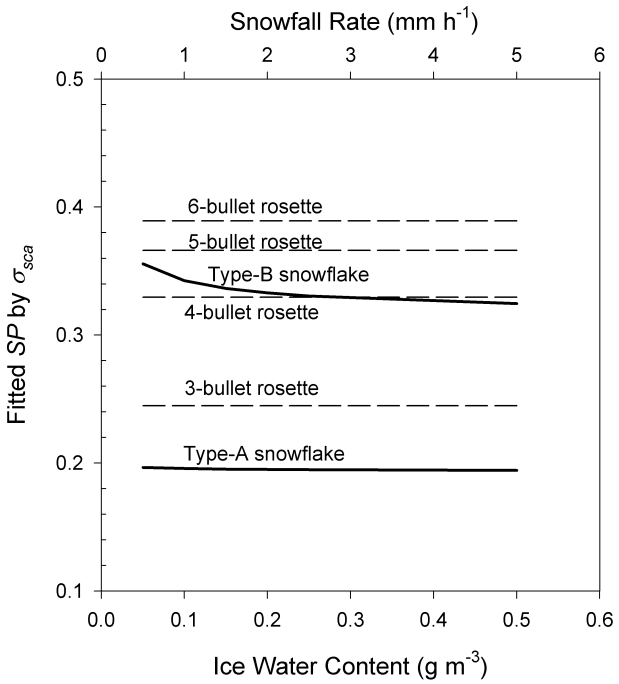

FIG. 10. Best-fit SP values concerning volume scattering coefficient σ_{sca}. A gamma size distribution with slope and dispersion parameters given by Heymsfield et al. (2002a) for temperature of -10°C is used for the rosettes. The size distribution given by Sekhon and Srivastava (1970) is used for snowflakes.

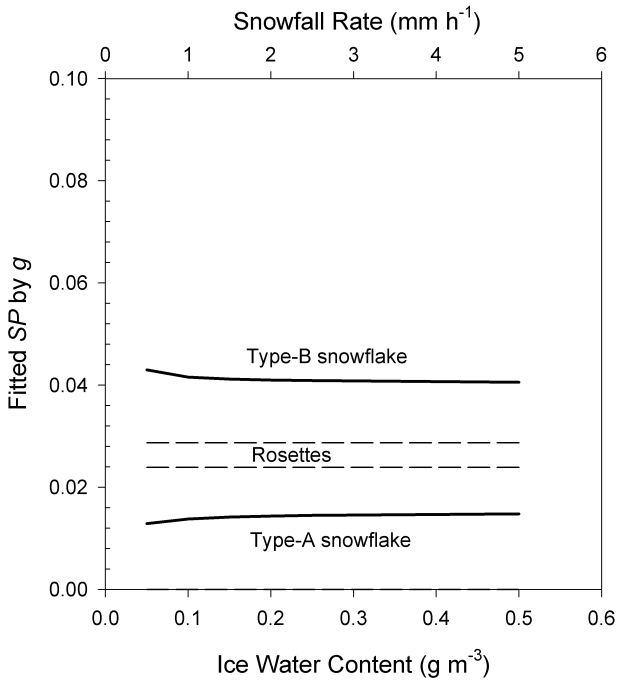

FIG. 11. Same as Fig. 10, except that the best-fit is for volume-averaged asymmetry parameters.

In the tropical ice cloud case, we assume a tropical standard atmosphere and an ice layer between 5 and 7 km over ocean. No liquid water cloud and rainfall are included. The ice particle size distribution is based on Heymsfield et al. (2002a). The calculated brightness temperatures at 150 GHz for a viewing zenith angle of 53° are shown in Fig. 13, varying ice water path from 0 to 1800 g m^{-2}. The results based on the solid- and the soft-sphere approximations are also shown for comparison. Since water vapor at the lower atmosphere in the Tropics masks most of the radiation from the surface, there is little difference between the vertically and horizontally polarized brightness temperatures. Therefore, only the vertical component is shown in this figure. Brightness temperatures decrease as ice water path increases. However, the rates of the decrease are significantly different depending on how the single scattering properties of the ice particles are calculated, with the largest rate for the solid-sphere approximation, the smallest rate for the soft-sphere approximation, and the rates based on the two approximations presented in this study are in between. The brightness temperatures based on the equal-mass sphere approximation agree within 3 K with those based on the polynomial fit approximation. So, the two proposed approximations yield similar accuracy in calculating brightness temperatures. The solid-sphere approximation causes significant underestimation, while the soft-sphere approximation causes significant overestimation of the brightness temperatures.

TABLE 1. The best-fit values of SP for volume-averaged scattering coefficients and asymmetry parameters. An ice water content of 0.2 g m^{-3} is used for rosettes and a snowfall rate of 2 mm h^{-1} is used for snowflakes in the size distributions.

Frequency (GHz)	Best-fit SP							
	Rosettes					Snowflakes		
	Three-bullet	Four-bullet	Five-bullet	Six-bullet	Average	Type-A	Type-B	Average
For volume-averaged scattering coefficients σ_{sca}								
85.5	0.46	0.54	0.58	0.59	0.54	0.25	0.40	0.33
150	0.25	0.33	0.37	0.39	0.36	0.20	0.33	0.27
220	0.17	0.25	0.29	0.32	0.26	0.16	0.27	0.22
For volume-averaged asymmetry parameter $\bar{g}$								
85.5	0.27	0.33	0.36	0.38	0.34	0.11	0.12	0.12
150	0.03	0.03	0.02	0.02	0.03	0.01	0.04	0.03
220	0.00	0.00	0.00	0.00	0.00	0.02	0.04	0.03

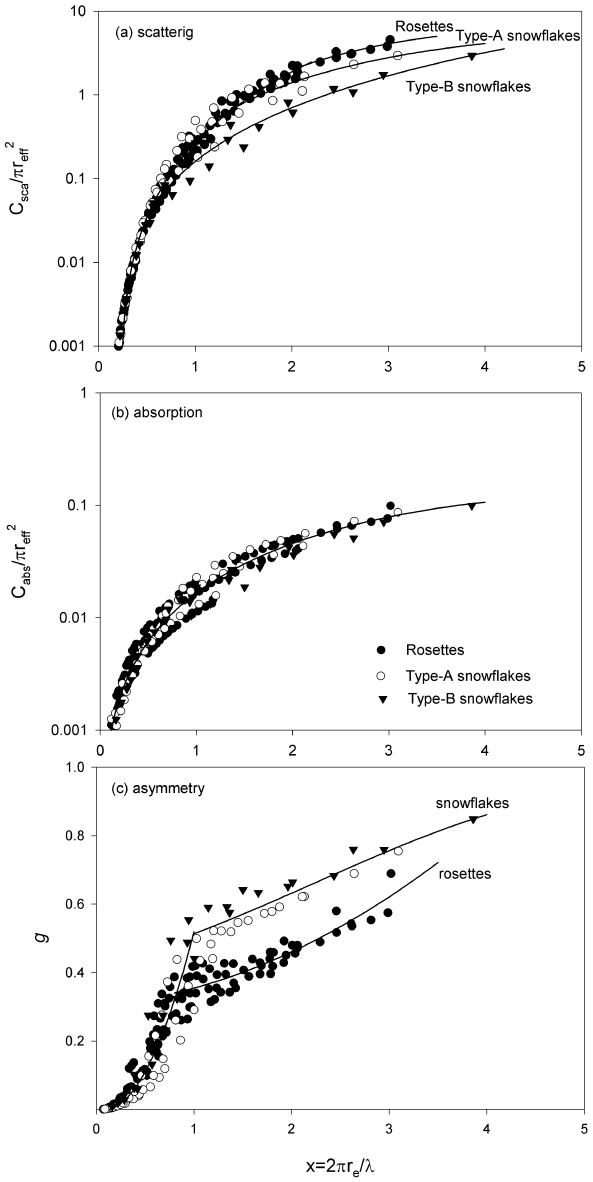

FIG. 12. Curve fitting to (a) $C_{sca}/\pi r_{eff}^2$, (b) $C_{abs}/\pi r_{eff}^2$, and (c) g for rosettes and snowflakes. The symbols are results from the DDA model. The lines are fitting curves using (9a) to (9c) with coefficients listed in Table 2.

For the snowfall case, an ocean surface with temperature of 5°C and a winter standard atmosphere at 45° latitude are used. The snow layer is assumed to be between surface and 5 km, with a constant snowfall rate layer below 3 km and linearly decreasing profile above. The snow consists of equally mixed type-A and type-B snowflakes. No liquid water cloud is included. The Sekhon and Srivastava (1970) size distribution is used for the snowflakes. The modeled brightness temperatures at 150 GHz are shown in Fig. 14 for a viewing zenith angle of 53°. It is seen that the solid- and the soft-sphere approximations result in very different brightness temperatures, even a different trend for the horizontally polarized brightness temperatures. The brightness temperatures calculated using the two approximations proposed in this study, agreeing with each other within 2K, are between those calculated by using the solid- and the soft-sphere approximations.

The findings from the above two cases are consistent with the results of the DDA modeling performed in section 2. That is, the solid-sphere approximation results in a too strong scattering, while the soft-sphere approximation causes the scattering intensity to be too weak. Consequently, neither of them can produce reasonable brightness temperatures at the high microwave frequencies. Additionally, the asymmetry parameter also plays a role in determining the modeled brightness temperatures. However, it is not clear how much the newly developed approximation for asymmetry parameter increases (decreases) the brightness temperatures relative to those of solid spheres (soft spheres). In conclusion, the approximations developed in this study are very useful for modeling high-frequency microwave radiances with a reasonable accuracy while keeping the computations efficient.

6. Conclusions

As high-frequency microwave data from satellite and airborne observations became available for retrieving ice water path and snowfall rate, there are increasing demands for a better method to calculate the complicated scattering properties of nonspherical ice and snow particles for these frequencies. This study proposes two approximation methods based on DDA modeling results. In designing the particle shapes in the DDA calculations, we take advantage of the recently published results on the relations among particle area ratio, density, and maximum dimension, which were derived from in situ measurements during many field experiments. The strategy of the approximations is to develop a method that is accurate while still having good computational efficiency.

Due to their complexity in shape and orientation, in many physical retrieval algorithms, ice and snow particles have so far been treated as equal-mass spheres of either solid ice (solid spheres) or a mixture of ice and air with a diameter equaling the particle's maximum dimension (soft spheres). The DDA modeling results of the present study indicated that neither of the two is a good approximation for the frequency range of 85 to 220 GHz. By analyzing the DDA model results, it is noticed that the scattering and absorption cross sections and the asymmetry parameter of the nonspherical particles have magnitudes between those of the imaginary equal-mass solid and soft sphere for the frequency range considered in this study. Therefore, our first parameterization is to approximate the single scattering properties of a nonspherical particle by an equal-mass sphere's. The diameter of this equal-mass sphere D is

TABLE 2. Coefficients for $C_{sca}/\pi r_{eff}^2$, $C_{abs}/\pi r_{eff}^2$, and g in (9a) to (9c).

$C_{SCO}/\pi r_{eff}^2$		a_1	a_2	a_3
Rosettes				
$x \le 2.2$		−0.36379E−01	0.11716E+00	0.18637E+00
$x > 2.2$		−0.60643E+00	0.10934E+01	−0.14630E+00
Type-A snowflakes				
$x \le 1.4$		−0.36379E−01	0.11716E+00	0.18637E+00
$x > 1.4$		−0.16220E+00	0.56253E+00	−0.66369E−01
Type-B snowflakes				
$x \le 0.5$		−0.36379E−01	0.11716E+00	0.18637E+00
$x > 0.5$		−0.96948E−02	0.15898E+00	0.10780E−01
$C_{abs}/\pi r_{eff}^2$		b_1	b_2	b_3
		0.74460E−02	0.10607E−01	−0.14505E−02
g	c_0	c_1	c_2	c_3
Rosettes				
$x \le 1.0$	0.0	−0.77361E−01	0.59902E+00	−0.18825E−02
$x > 1.0$	0.30617E+00	0.19795E−01	0.29307E−01	−0.29968E−03
Snowflakes				
$x \le 1.0$	0.0	−0.77361E−01	0.59902E+00	−0.18825E−02
$x > 1.0$	0.42725E+00	0.62429E−01	0.28416E−01	−0.42245E−02

bigger than the diameter of the solid sphere D_0, but smaller than the particle's maximum dimension D_{max}. Defining a softness parameter, SP = $(D - D_0)/(D_{max} - D_0)$, it is found that the best-fit equal-mass sphere has an SP value of 0.2 ~ 0.5 for scattering coefficient, depending on frequency and particle shape. At 150 GHz, the best softness parameter is ~1/3 when averaging over all particle shapes. For the asymmetry parameter, SP = 0 is found to be a good approximation for frequencies higher than 150 GHz, while SP = 0.3 for rosettes and SP = 0.1 for snowflakes are suitable for 85.5 GHz. A list of the best-fit softness parameters for three different frequencies and six different particle shapes are given in Table 1.

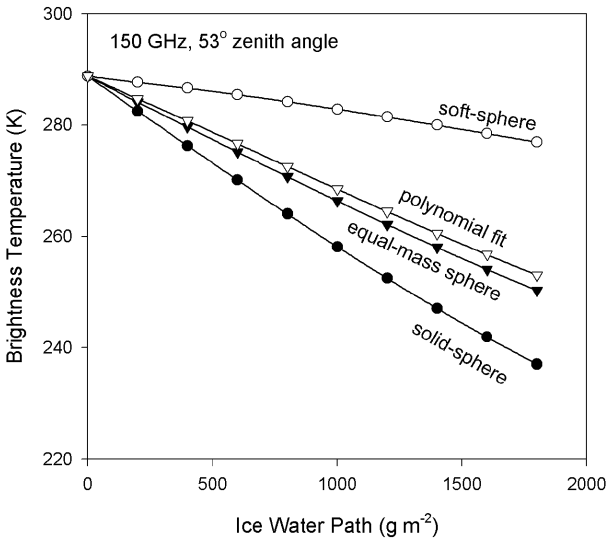

FIG. 13. Vertically polarized brightness temperatures simulated by a radiative transfer model for an ice cloud case. The two approximations proposed in this study are compared with the solid- and the soft-sphere approximations.

The second approximation is a polynomial fit to the scattering and absorption cross sections and the asymmetry parameter as a function of the particle size parameter defined by the effective radius and wavelength. For scattering, three fitting curves are derived, respectively, for rosettes, type-A snowflakes, and type-B snowflakes. For the absorption, a single curve is used to fit all particle shapes. For the asymmetry parameter, two fitting curves are used for rosettes and snowflakes, respectively. The coefficients of these fitting curves are listed in Table 2. The applicable ranges of these fitting curves are for frequencies from 85 to 220 GHz, and for size parameter less than 3 for rosettes and less than 4 for snowflakes.

Radiative transfer modeling is conducted using the proposed approximations for an ice cloud case and a snowfall case. The results show that the brightness temperatures based on the two proposed approximations agree with each other within 3 K, while they are largely different from those based on the solid- and the soft-sphere approximations. The soft-sphere approximation overestimates while the solid-sphere approximation underestimates the upwelling brightness temperatures.

This study emphasizes the scattering by large ice aggregates and snowflakes, to which the high-frequency microwave radiations have sufficient sensitivity. We assumed that there is no preferential orientation for these particles. Scattering from particles parallel to the horizontal plane was studied by Tang and Aydin (1995). However, to the author's knowledge, there is no observational evidence that large aggregates and snowflakes have a preferential orientation. To detect thin ice clouds with smaller ice crystals, observations at short wave-

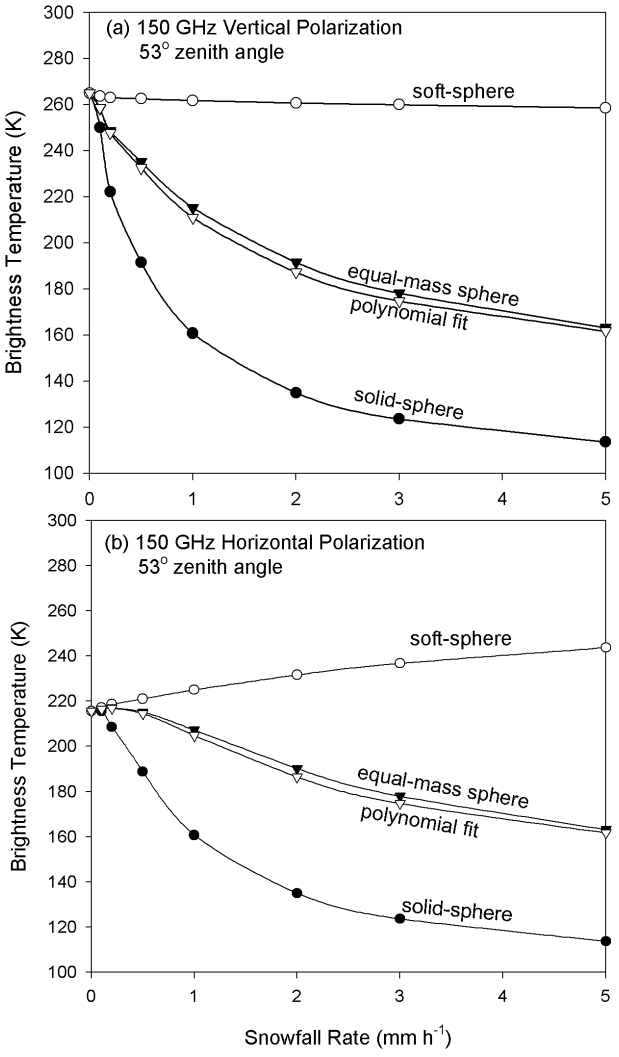

FIG. 14. (a) Vertically and (b) horizontally polarized brightness temperatures simulated by a radiative transfer model for a snowfall case. The two approximations proposed in this study are compared with the solid- and the soft-sphere approximations.

lengths, for example, submillimeter waves (Evans et al. 2002), far-infrared (Yang et al. 2003), or visible/infrared (Liou et al. 1990; Minnis et al. 1993) are more preferable. The high microwave frequencies investigated in this study are suitable for thick ice cloud decks and solid precipitations.

Acknowledgments. The author is very grateful to Drs. B. T. Draine and P. J. Flatau for providing their well-documented DDA model. Comments and suggestions from three anonymous reviewers are very helpful. This research has been supported by DOE ARM Grant DE-FG02-03ER63526 and NASA Grant NNG04GB04G.

REFERENCES

Bennartz, R., and G. W. Petty, 2001: The sensitivity of microwave remote sensing observations of precipitation to ice particle size distributions. *J. Appl. Meteor.,* **40,** 345–364.

Bohren, C. F., and L. J. Battan, 1982: Radar backscattering of microwaves by spongy ice spheres. *J. Atmos. Sci.,* **39,** 2623–2628.

Deeter, M. N., and K. F. Evans, 2000: A novel ice-cloud retrieval algorithm based on the Millimeter-Wave Imaging Radiometer (MIR) 150- and 220-GHz channels. *J. Appl. Meteor.,* **39,** 623–633.

Draine, B. T., 1988: The discrete-dipole approximation and its application to interstellar graphite grains. *Astrophys. J.,* **333,** 848–872.

——, and J. Goodman, 1993: Beyond Clausius–Mossotti: Wave propagation on a polarizable point lattice and the discrete dipole approximation. *Astrophys. J.,* **405,** 685–697.

——, and P. J. Flatau, 1994: Discrete-dipole approximation for scattering calculations. *J. Opt. Soc. Amer.,* **11A,** 1491–1499.

——, and ——, 2000: User guide for the discrete dipole approximation code DDSCAT (version 5a10). Princeton University Observatory, 1–42. [Available online at http://arxiv.org/abs/astro-ph/0008151v4.]

Evans, K. F., and G. L. Stephens, 1995: Microwave radiative transfer through clouds composed of realistically shaped ice crystals. Part I: Single scattering properties. *J. Atmos. Sci.,* **52,** 2041–2057.

——, S. J. Walter, A. J. Heymsfield, and M. N. Deeter, 1998: Modeling of submillimeter passive remote sensing of cirrus clouds. *J. Appl. Meteor.,* **37,** 184–205.

——, ——, ——, and G. M. McFarquhar, 2002: Submillimeter-wave cloud ice radiometer: Simulations of retrieval algorithm performance. *J. Geophys. Res.,* **107,** 4028, doi:10.1029/2001JD000709.

Grenfell, T. C., and S. G. Warren, 1999: Representation of a nonspherical ice particle by a collection of independent spheres for scattering and absorption of radiation. *J. Geophys. Res.,* **104,** 31 697–31 709.

Henyey, L. C., and J. L. Greenstein, 1941: Diffuse radiation in the galaxy. *Astrophys. J.,* **93,** 70–83.

Heymsfield, A. J., and L. M. Miloshevich, 2003: Parameterizations for the cross-sectional area and extinction of cirrus and stratiform ice cloud particles. *J. Atmos. Sci.,* **60,** 936–956.

——, A. Bansemer, P. R. Field, S. L. Durden, J. L. Stith, J. E. Dye, W. Hall, and C. A. Grainger, 2002a: Observations and parameterizations of particle size distributions in deep tropical cirrus and stratiform precipitating clouds: Results from in situ observations in TRMM field campaigns. *J. Atmos. Sci.,* **59,** 3457–3491.

——, S. Lewis, A. Bansemer, J. Iaquinta, L. M. Miloshevich, M. Kajikawa, C. Twohy, and M. R. Poellot, 2002b: A general approach for deriving the properties of cirrus and stratiform ice cloud particles. *J. Atmos. Sci.,* **59,** 3–29.

Kajikawa, M., 1982: Observations of the falling motion of early snowflakes. Part I: Relationship between the free-fall pattern and the number and shape of component snow crystals. *J. Meteor. Soc. Japan,* **60,** 797–803.

——, and A. J. Heymsfield, 1989: Aggregation of ice crystals in cirrus. *J. Atmos. Sci.,* **46,** 3018–3121.

Katsumata, M., H. Uyeda, K. Iwanami, and G. Liu, 2000: The response of 36- and 89-GHz microwave channels to convective snow clouds over ocean: Observation and modeling. *J. Appl. Meteor.,* **39,** 2322–2335.

Liou, K. N., S. C. Ou, Y. Takano, F. P. J. Valero, and T. P. Ackerman, 1990: Remote sensing of the tropical cirrus cloud temperature and optical depth using 6.5- and 10.6-micron radiometers during STEP. *J. Appl. Meteor.,* **29,** 716–726.

Liu, G., 1998: A fast and accurate model for microwave radiance calculations. *J. Meteor. Soc. Japan,* **76,** 335–343.

——, and J. A. Curry, 1997: Precipitation characteristics in the GIN Seas determined using satellite microwave data. *J. Geophys. Res.,* **102,** 13 987–13 997.

——, and ——, 2000: Determination of ice water path and mass median particle size using multichannel microwave measurements. *J. Appl. Meteor.,* **39,** 1318–1329.

Magono, C., and T. Nakamura, 1965: Aerodynamic studies of falling snowflakes. *J. Meteor. Soc. Japan,* **43,** 139–147.

Minnis, P., K. N. Liou, and Y. Takano, 1993: Inference of cirrus cloud properties using satellite-observed visible and infrared radiances. Part I: Parameterization of radiance field. *J. Atmos. Sci.,* **50,** 1279–1304.

Mishchenko, M. I., L. D. Travis, and D. W. Mackowski, 1996: T-Matrix computations of light scattering by nonspherical particles: A review. *J. Quant. Spectrosc. Radiat. Transfer,* **55,** 535–575.

——, W. J. Wiscombe, J. W. Hovnier, and L. D. Travis, 2000: Overview of scattering by nonspherical particles. *Light Scattering by Nonspherical Particles: Theory, Measurements, and Applications,* M. I. Mishchenko, J. W. Hovnier, and L. D. Travis, Eds., Academic Press, 29–60.

O'Brien, S. G., and G. H. Goedecke, 1988: Scattering of millimeter waves by snow crystals and equivalent homogeneous symmetric particles. *Appl. Opt.,* **27,** 2439–2444.

Purcell, E. M., and C. R. Pennypacker, 1973: Scattering and absorption of light by nonspherical dielectric grains. *Astrophys. J.,* **186,** 705–714.

Racette, P., R. F. Adler, J. R. Wang, A. J. Gasiewski, D. M. Jackson, and D. S. Zacharias, 1996: A millimeter-wave imaging radiometer for cloud, precipitation and atmospheric water vapor studies. *J. Atmos. Oceanic Technol.,* **13,** 610–619.

Schols, J. L., J. A. Weinman, G. D. Alexander, R. E. Stewart, L. J. Angus, and A. C. L. Lee, 1999: Microwave properties of frozen precipitation around a North Atlantic cyclone. *J. Appl. Meteor.,* **38,** 29–43.

Sekhon, R. S., and R. C. Srivastava, 1970: Snow size spectra and radar reflectivity. *J. Atmos. Sci.,* **27,** 299–307.

Tang, C., and K. Aydin, 1995: Scattering from ice crystals at 94 and 220 GHz millimeter wave frequencies. *IEEE Trans. Geosci. Remote Sens.,* **33,** 93–99.

Vivekanandan, J., J. Turk, and V. N. Bringi, 1991: Ice water estimation and characterization using passive microwave radiometry. *J. Appl. Meteor.,* **30,** 1407–1421.

Wang, J. R., G. Liu, J. D. Spinhirne, P. Racette, and W. D. Hart, 2001: Observations and retrievals of cirrus cloud parameters using multichannel millimeter-wave radiometric measurements. *J. Geophys. Res.,* **106,** 15 251–15 263.

Wang, P. K., 1997: Characterization of ice crystals in clouds by simple mathematical expressions based on successive modification of simple shapes. *J. Atmos. Sci.,* **54,** 2035–2041.

Weng, F., and N. C. Grody, 2000: Retrieval of ice cloud parameters using microwave imaging radiometer. *J. Atmos. Sci.,* **57,** 1069–1081.

Yang, P., and K. N. Liou, 1996: Finite-difference time domain method for light scattering by small ice crystals in three-dimensional space. *J. Opt. Soc. Amer.,* **13A,** 2072–2085.

——, and ——, 1998: An efficient algorithm for truncating spatial domain in modeling light scattering by finite-difference technique. *J. Comput. Phys.,* **140,** 346–369.

——, and Coauthors, 2003: Spectral signature of ice clouds in the far-infrared region: Single-scattering calculations and radiative sensitivity study. *J. Geophys. Res.,* **108,** 4569, doi:10.1029/2002JD003291.

Zhao, L., and F. Weng, 2002: Retrieval of ice cloud parameters using the Advanced Microwave Sounding Unit. *J. Appl. Meteor.,* **41,** 384–395.